Science
AAAS

Supplementary Materials for

ATP-dependent force generation and membrane scission by ESCRT-III and Vps4

Authors: Johannes Schöneberg[1,2,3], Mark Remec Pavlin[2,4§], Shannon Yan[1,2,5§], Maurizio Righini[6†], Il-Hyung Lee[1,2†], Lars-Anders Carlson[1,2†], Amir Houshang Bahrami[3], Daniel H. Goldman[1,2,5†], Xuefeng Ren[1,2], Gerhard Hummer[3,7], Carlos Bustamante[1,2,4,5,6,8,9*] and James H. Hurley[1,2,4,9*]

§Equal contribution

*Correspondence to: James H. Hurley jimhurley@berkeley.edu or Carlos Bustamante carlosb@berkeley.edu

This PDF file includes:

Other Supplementary Materials for this manuscript include the following:

Materials and Methods:

Protein expression, purification and labeling

The following proteins were expressed as N-terminal TEV-cleavable His_6-MBP fusion constructs: Snf7 (N-cys, indicating a cysteine inserted in between the TEV site and the initial methionine), Vps2 (wt and N-cys) and Vps24 (wt and N-cys). Proteins were expressed in *E. coli* Rosetta2 (DE3) cells at 20°C overnight in LB medium. Cell pellets were frozen and stored until use. Pellets were resuspended in Buffer NiW (300 mM NaCl, 50 mM Tris HCl pH 7.4, 10 mM imidazole, 2 mM β-mercaptoethanol (βME)), sonicated, and centrifuged. The supernatant was applied to a gravity column containing 8 ml pre-equilibrated Ni-NTA resin. After washing with NiW buffer, the sample was eluted in 10 ml NiE Buffer (300 mM NaCl, 50 mM TrisHCl pH 7.4, 300 mM imidazole). The eluate was immediately applied to a HiLoad 16/60 Superdex 200 (GE Healthcare, Chicago, IL, USA) chromatography column in buffer S200 (100mM NaCl, 50 mM TrisHCl pH 7.4, 0.1 mM TCEP). Fractions with the highest 280nm absorption were pooled to a total volume of 6 ml and concentration determined from its absorption at 280 nm (NanoDrop spectrophotometer, Thermo Fisher Scientific, Waltham, MA, USA).

Labeling was performed by adding 1.5 x molar excess dye (Atto 488 maleimide, Attotec GmbH or Lumidyne 550, Lumidyne Technologies) to the pooled fractions and incubating overnight at 4˚C. As MBP contains no cysteine, only proteins of the ESCRT module were labeled by the dyes. The following day, the reaction was incubated for 2 h at room temperature with TEV protease (0.65 mg/ml final concentration) and then applied on a HiLoad 16/60 Superdex 75 (GE Healthcare) chromatography column in buffer S75 (300 mM NaCl, 50 mM TrisHCl pH 7.4, 0.1 mM TCEP). The two purest fractions were selected based on SDS-PAGE, read both with a Typhoon for dye absorbance and Coomassie staining, and the concentration determined by Nanodrop. Finally, 3 mM sodium azide was added. Snf7 was always prepared fresh, stored at 4˚C and used within 14 days. Vps2 and Vps24 eluates from the Ni-NTA gravity column were incubated with TEV protease (0.65 mg/ml final concentration) for 2 h at room temperature and then immediately applied to a HiLoad 16/60 Superdex 75 (GE Healthcare) chromatography column in buffer S75 (Fig. S1). The purest fractions were pooled and concentrated to stocks of 100-200 μM final concentration, aliquoted, flash frozen in liquid nitrogen and stored at -80˚C until use. For labeling, aliquots were incubated with 2 x molar excess dye (Atto 488 maleimide, Attotec GmbH or Lumidyne 650, Lumidyne Technologies) at 4˚C overnight and desalted with a S75 buffer equilibrated spin column (Biorad) in S75 Buffer.

Vps4 (wt and mutants) was expressed as N-terminal TEV-cleavable His_6 fusion construct. Expression and Ni-NTA steps were done as described above. The Ni-NTA eluate was loaded on a 5 ml HiTrap Q Sepharose Column (GE Healthcare) and eluted with a 0-100% gradient in 12 column volumes from buffer A (50 mM NaCl, 20 mM TrisHCl pH 8.0, 0.1mM TCEP) to buffer B (500 mM NaCl, 20mM TrisHCl pH 8.0, 0.1mM TCEP). The single Vps4 peak was identified by its absorption at 280 nm, pooled and further purified on a HiLoad 16/60 Superdex 75 (GE Healthcare) chromatography column in buffer S75. Vps4 was concentrated to 100 μM, aliquoted and flash frozen in liquid N_2 and stored at -80˚C until use.

Preparation of GUVs

Lipids were purchased from Avanti Polar Lipids (Alabaster, AL). Stock solutions of 10 mg/ml (or lower for the trace components) were prepared by dilution with chloroform. Lipids were mixed at a ratio of 79.1% palmitoyloleoyl-phosphatidylcholine (POPC), 20.5% palmitoyloleoyl-

phosphatidylserine (POPS), 0.2% TopFluor-PS or 0.3% dioleoyl-phosphatidylethanolamine (DOPE)-Atto647 (Atto-Tec GmbH) and 0.1 % distearoyl-phosphatidylethanolamine (DSPE)-PEG(2000)-Biotin. 50 µl of the mixture at 3 mg/ml was thinly spread on indium tin oxide (ITO) coated glass slides (Sigma Aldrich). The lipid film was dried for 1 h in a vacuum chamber before being rehydrated in formation buffer. The formation buffer was composed of 150 mM NaCl, 25 mM Tris HCl pH 7.4, 0.05 mM TCEP, 262 mM sucrose. $MgCl_2$ and NPE-caged ATP (adenosine 5'-triphosphate, P3-(1-(2-nitrophenyl)ethyl) ester, disodium salt, Life Technologies) were added to a final concentration of 2 mM. Double distilled H_2O or NaCl were carefully added in trace amounts to reach a total osmolarity of 580 mOsm. For encapsulation at physiological ionic strength (*35*), purified proteins in buffer were added to reach the following final concentrations: Snf7 2µM, Vps2 2µM, Vps24 2µM and Vps4 2.6µM for the high concentration experiments, each component 10x lower for the low concentration experiments. GUVs were electroformed over 1 h on ice. For all experiments, GUVs were diluted with Buffer S75 at least 1:50.

High precision optical tweezers force measurements

A laser trap on the "mini-tweezers" (Steve B. Smith Engineering, Los Lunas, New Mexico) was formed by focusing two counterpropagating laser beams (λ = 830 nm) through two opposite objective lenses. The force exerted by the nanotube onto a micron-size polystyrene bead trapped by the tweezers was measured by the extent that the laser beams are refracted upon passing through the bead, which were detected by pairs of position sensitive detectors (PSDs). Experiments were performed inside a microfluidic chamber (Fig. S2C) that comprises three channels (top, bottom, and main). Channels were cut into a double layer of plastic film (Nescofilm), which is melted to seal between two microscope cover slides on a hotplate. The channels were connected via glass capillary tubes (i.e. dispenser tubes; King Precision Glass, Claremont, CA, USA). Six holes were drilled into the top cover slide via a laser cutter to allow connection of inlet and outlet tubing to each channel.

We injected 1.56 µm streptavidin-coated beads (Spherotech, Lake Forest, IL, USA) and biotinylated lipid vesicles respectively from the top and bottom channels. At the outlet of the dispenser tubes into the main channel, we trapped individual beads and vesicle and configure them into tube pulling geometry (*36*) inside the main observation channel (Fig. 1A). An aspiration micro-pipette positioned in the main channel was connected to a high precision pressure controller (MFCS-EZ, 0 to -69 mbar, Fluigent, Villejuif, France), which we use to immobilize a single vesicle on the micro-pipette tip via precise suction control. To release NPE-caged ATP encapsulated inside the vesicle via light activation, we coupled a UV light emitting diode (LED) (Thorlabs, Newton, NJ, USA, λ = 340 nm) to a solarization-resistant multimode optical fiber (Thorlabs) placed right next to the micro-pipette inside the fluidic chamber. We carefully positioned the fiber in such a way that the light cone exiting the fiber (Numerical Aperture 0.22) directly illuminates the vesicle immobilized on the pipette tip (Fig. 1B).

Combined confocal imaging and optical tweezing

We integrated a single optical trap for tweezing onto a commercial confocal imaging system, which we refers to a "Confleezers" (Fig. S2A). The platform was constructed on an inverted microscope unit (motorized Ti-E, Nikon) that contains a stage raiser and an additional (upper) filter cube turret to accommodate and direct the high-power IR laser for trapping. The lower (standard) filter cube turret houses imaging wavelength filters. A Nikon A1R resonant scanning confocal unit was attached to the left camera port of the microscope body. Four solid state lasers

(405, 488, 561, 640 nm; LU-N4, Nikon) were paired with appropriate emission filters for fluorescence imaging excitation. A high speed sCMOS camera (ORCA-Flash 4.0 LT, Hamamatsu Photonics) for fast imaging and real-time monitoring of sample manipulation was attached to the right camera port of the scope body and customized to accommodate an IR filter for imaging while trapping. Bright field illumination was provided by the top condenser unit. Wide field fluorescence imaging light was provided from the back side of the microscope (Sola SE II 365, Lumencor). The optical trap was formed by a 5W 1070 nm IR laser (YLR-5-1070-Y12, IPG Photonics). The IR laser's optical fiber output was connected to a laser beam steering optics unit (customized, mirror adjustment and lens collimation units, in parts based on E3300, Elliot Scientific) which was attached to the back side of the scope body through the upper turret. An IR dichroic mirror (Z1064RDC-SP, Chroma) directed the laser to the objective back aperture. The scope was equipped with a full set of objectives with various magnifications from 10x to 100x.

To form an optical trap at the z-center of the fluidic chamber (i.e. away from the coverslip surface where hydrodynamic interfere is known to compromise the precision of force measurements), an objective with long enough working distance was needed; here we used the Plan Apochromat 60x/1.2NA Water Immersion Objective (MRD07602, Nikon). The position of optical trap z-focus was further carefully aligned to match the z-focus of the scanning confocal unit. A quadrant photodiode (QPD) system (E4100, Elliot Scientific) was attached to the top condenser unit to collect position information of the trapped bead. The refracted IR light from trapped bead was steered and focused on the QPD. QPD voltage outputs were then converted to trapping forces in real time using a custom written software that combines LabView for PC-to-instrument communication and an underlying Python layer for signal processing. Trap stiffness was calculated using the power spectra of position fluctuations of the trapped bead. Imaging is controlled by the imaging software NIS-Elements (Nikon).

The microscope was maintained in a room designed to minimize and to attenuate mechanical and acoustic vibration. A 4' x 6' x 8" tapped optical table (TMC) and a custom-built scope enclosure were used to optimize the stability of our experimental setup. A high-precision xyz piezo stage system (P-545K003, Physik Instrumente GmbH & Co. KG) was installed on top of the general use motorized stage (Ti-S, Nikon) to aide fine manipulation of samples. The stage was machined to accommodate the same microfluidic chambers used in the mini-tweezers (three channels, glued micropipette, and UV optical fiber, see above). Experiments were carried out at room temperature.

Image and data analysis

A baseline recording preceded every force measurement. A linear fit (custom made Python code) was used to capture small drifts in force (due to e.g. immersion water evaporation and resulting coverslip bending relaxation) that were then subtracted from the force trajectory. See supporting information (Fig. S3) for membrane parameter calculation. Confocal image stacks of membrane tubes were processed with a suite of custom-made Python scripts as follows: The signal to noise ratio was first improved by applying a walking average over a 20 frame window to the recorded raw data (recorded at 3 frames / s). After bleaching correction, the tube vector (vector between the attachment points on bead and vesicle) was calculated using brightfield and membrane channel for attachment point detection (Fig. S4A-D). The tube fluorescence intensity was then obtained by fitting a Gaussian to the averaged histogram of the diffraction. Quantitation of tube protein fluorescence is based on the known protein concentration in the GUV lumen from

which a conversion factor of fluorescence intensity to protein copy number was derived (see Fig. S4F-H). Tube radius was determined based on the tube's fluorescence intensity using a calibration from tubes of known radius (*36*). For puncta classification, the standard deviation of the background intensity σ_{bg} of the protein channels was calculated and compared with the peak fluorescence intensity of a puncta candidate. A puncta was counted if it was at least 5 pixels wide and its intensity maximum > 7 σ_{bg}.

Relation between the radius of a membrane tube under tension and the pulling force

According to the model of Derenyi et al. (*37*), which is based on Helfrich's membrane elastic theory, the free energy of a cylindrical membrane tube of radius r and length L under tension σ subject to a pulling force f is

$$G(r, L) = \left(\frac{\kappa}{2r^2} + \sigma\right) 2\pi r L - fL\,,$$

where κ is the membrane bending rigidity and the pressure-volume term has been neglected. Tension and pulling force are balanced if $\partial G/\partial r = \partial G/\partial L = 0$, which defines the equilibrium radius r_0 and force f_0,

$$r_0 = \sqrt{\frac{\kappa}{2\sigma}}, \qquad f_0 = 2\pi\sqrt{\kappa\sigma}\,.$$

If the radius r of the tube deviates from r_0, the force f required to balance the tension is given by $\partial G/\partial L = 0$. By using the relations for r_0 and f_0 and after some rearrangements, one obtains the following expression for the force:

$$\frac{f}{f_0} = \frac{1}{2}\left(\frac{r}{r_0} + \frac{r_0}{r}\right).$$

This relation can be inverted to obtain an expression for the tube radius as a function of the force,

$$\frac{r}{r_0} = \frac{f}{f_0} - \sqrt{\frac{f^2}{f_0^2} - 1}\,.$$

We conclude that any deviation of the tube radius r from r_0 is associated with an increase in the force.

Supplementary Figures

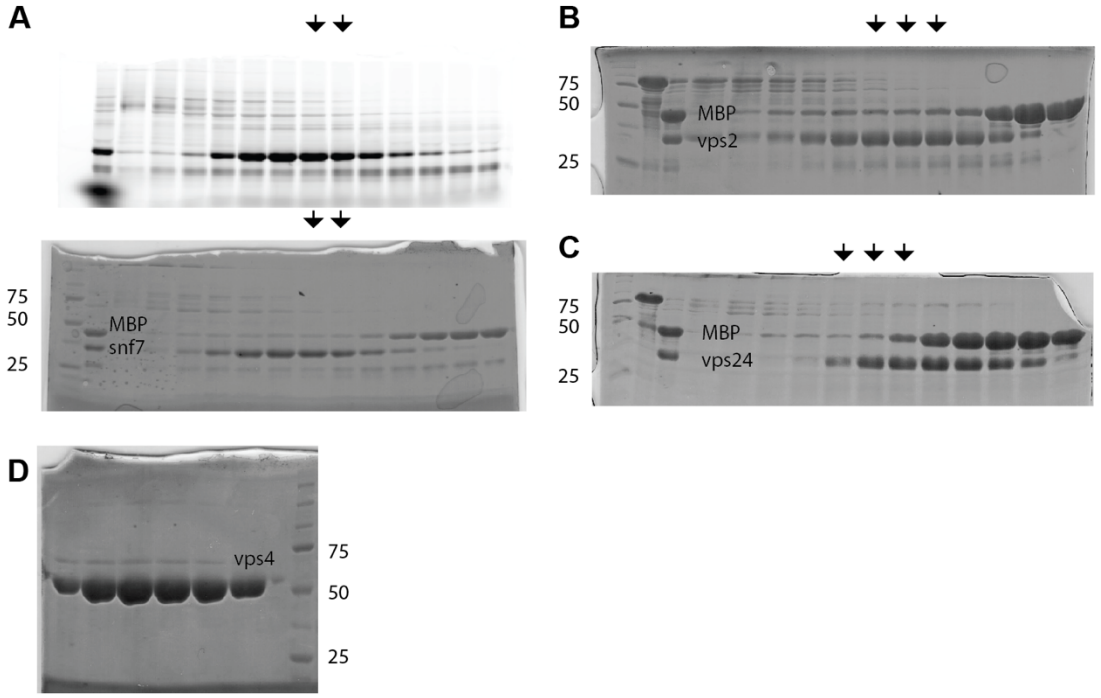

Fig. S1. **Protein purification.** A. Cy3B labeled Snf7 after FPLC fractionation on Superdex 75, Typhoon fluorescence scan (top) and Coomassie stain (bottom). B. Coomassie of Vps2 after FPLC fractionation on Superdex 75. C. Coomassie of Vps24 after FPLC fractionation on Superdex 75. D. Coomassie of Vps4 after FPLC fractionation on Superdex 75. Except Vps4, all proteins were expressed as MBP fusion constructs to facilitate expression.

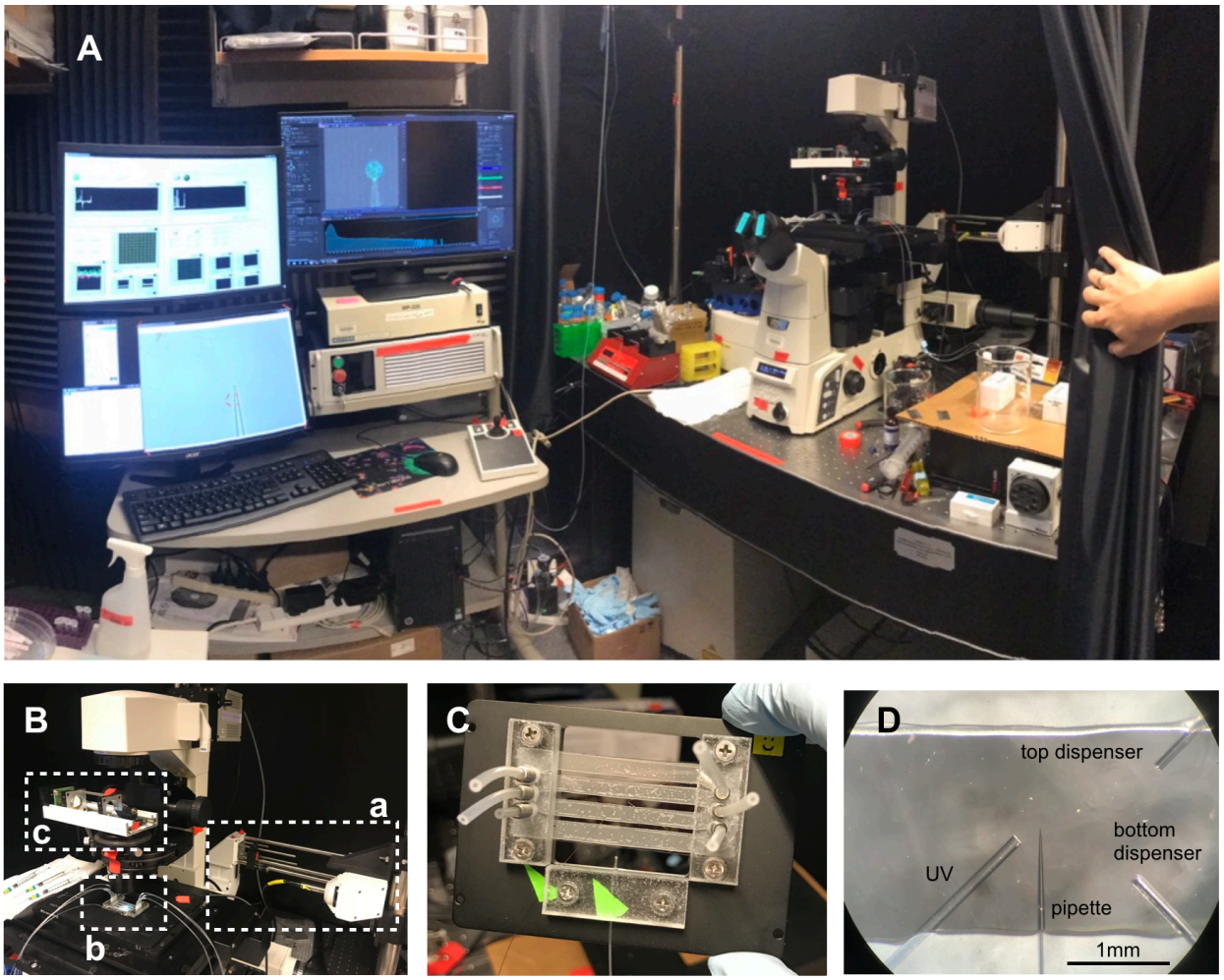

Fig. S2: **Confleezers setup and microfluidic chamber**. A, The "Confleezers" combines confocal microscopy, an optical tweezer and microfluidics in one setup. B, The trap was produced by focusing an IR laser into a high NA, 60x water immersion objective (inset a). The sample was placed in a microfluidics chamber (inset b) to ensure extended time optical tweezing in a debris free environment. Optical trap calibration and force readout was accomplished via back focal plane illumination of a quadrant photodiode (inset c). C. The microfluidics chamber has three fluid inlets (left), three fluid outlets (right) a fixed UV fiber (bottom left) and a fixed aspiration pipette (bottom right). D. Zoom into the center of the middle channel of the microfluidics chamber. The chamber minimized experimental perturbation by separating pulling beads (top channel) and vesicles (bottom channel) from the main channel (middle). Small dispenser tubes connected the top and bottom channel to the main and delivered beads and vesicles individually into the main experimental channel where they were picked up with the trap. Scale bar: 1mm.

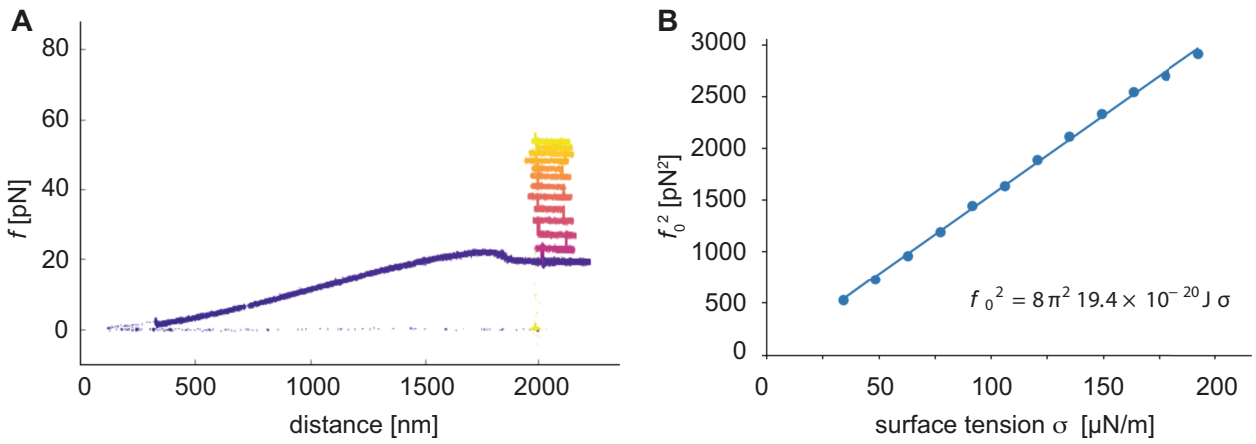

Fig. S3: **Membrane bending rigidity determination.** A. A typical tube pulling trace for an empty (no ESCRTs encapsulated) GUV (time in color from blue, early to yellow, late). First the vesicle was approached with the pulling bead (right to left dots on the bottom). Upon touching the surface, pulling on the membrane generated a force (blue line from left to right) as the vesicle was pulled. Above a certain threshold in force a tube was pulled out of the vesicle (hump in the blue curve) and the tube was extended with constant force $f_0 = 20pN$. While maintaining a tube, increasing the pipette suction increased the vesicle surface tension, leading to a higher tube force $\overline{f_0} > f_0$. The figure depicts the sampling of increasing suction values and its effect on the tube force (colored vertical lines). B. The characteristic tube force profile behavior was recorded as the suction pressure was varied. Using the relation $f_0 = 2\pi\sqrt{2\kappa\sigma}$, the bending rigidity κ was determined by fitting. The relation $r_0 = \sqrt{\kappa/2\sigma}$ then gives the corresponding membrane nanotube radius.

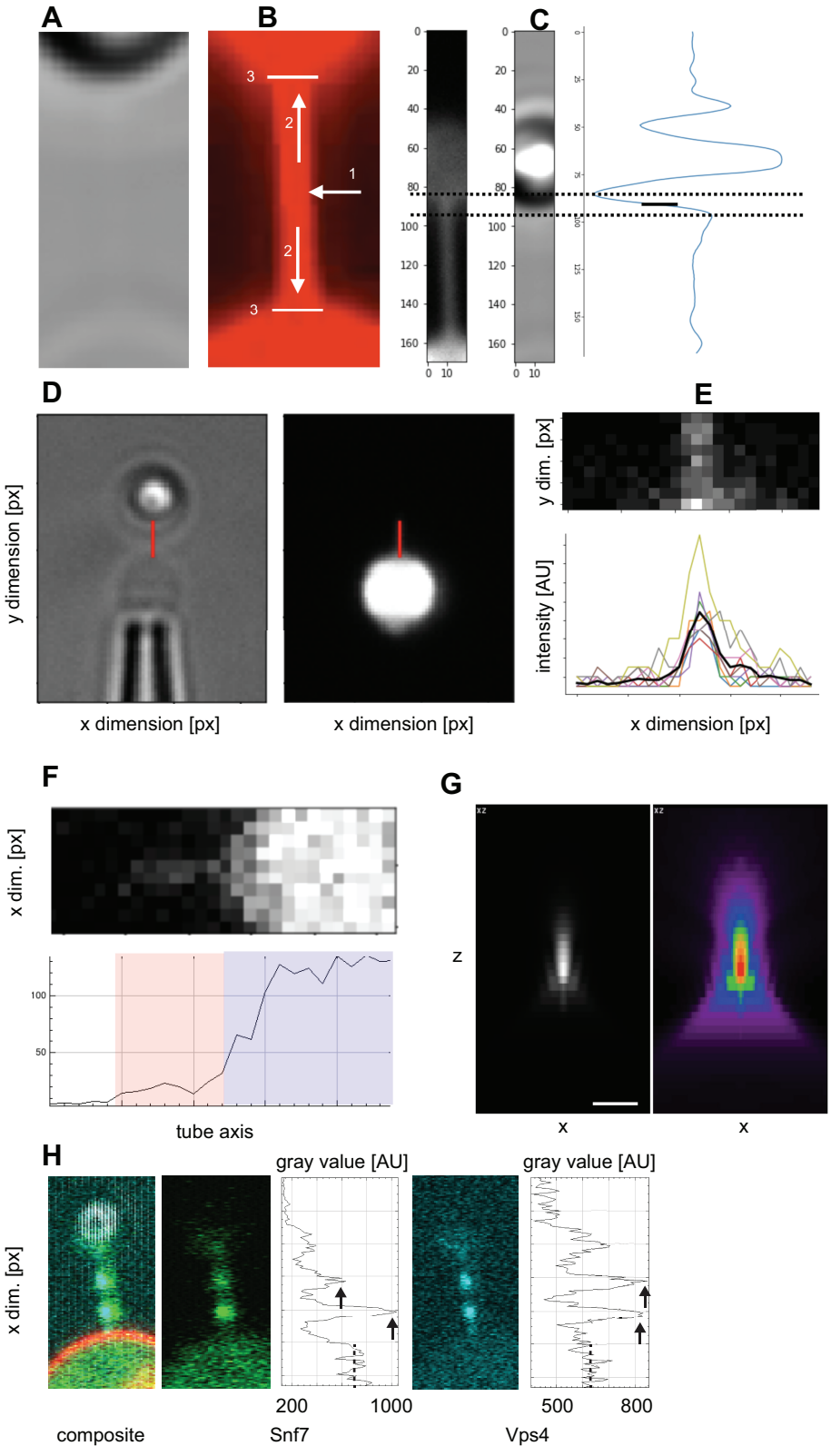

Fig. S4: Tube vector detection and intensity calculation. For every movie frame, the brightfield channel (A) and the membrane channel (B) were used for vector calculation. In the membrane

channel (B), first, the mid-point of the tube (arrow 1) was found. From there, the length of the tube vector was grown (arrows 2) until the bead or vesicle membrane was reached respectively (arrows 3). C. The position of the bead was determined from the brightfield channel. Along the tube axis, the grey value of the bead showed a characteristic signal. The midpoint (solid line) between the first grey value maximum and first the grey value minimum (dashed lines) was defined as the boundary of the bead. D. The boundary of the bead was found in the grey value histogram as the midpoint between the first minimum and the baseline. The resulting tube vector was plotted over the brightfield (left) and membrane channel (right). E. As a diffraction limited line, the tube intensity was calculated by averaging the tube intensity histograms perpendicular to the tube vector (colored) and fitting the resulting histogram (black) with a Gaussian. F and G. Molecular copy number calculation were based on the known internal concentration of single-cysteine labeled proteins and their fluorescence intensity in the vesicle and the tube. F. For quantitation calibration, a rectangular box of the lumen of the GUV was used that is defined in x,y by the image section (F, top and bottom blue) and in z by the optical slice imaged (G) given numerical aperture NA = 0.9, index of refraction n = 1.33, excitation λ = 488 nm, pinhole diameter = 2 μm, and excitation full width half maximum in z = 2.85 μm. From the volume of this box and the protein concentration, the fluorescence intensity to copy number conversion factor was determined. This conversion factor was then used to determine the total number of protein molecules in the tube (F, bottom red) or the total number of protein molecules in a given punctum on the tube. H. Puncta (maxima in the intensity profile on the tube, black arrows) were quantitated based on the above conversion factor and the integrated fluorescence intensity of the puncta.

Supplementary Movies

Movie S1. Force generation by the ESCRT module. A GUV aspirated on a micropipette was approached by a bead held in an optical trap (mini-tweezers set-up). The bead was moved towards and then away from the membrane, extracting a membrane nanotube. Upon ATP release (t = 0 s) a retraction force is created that is so strong that the bead is pulled out of the trap towards the vesicle.

Movie S2. Visualization of a representative membrane scission event. A membrane nanotube was pulled out of a GUV within which the full ESCRT module had been encapsulated, measured in the Confleezers set-up. The tube behavior is displayed before and after ATP is uncaged by UV at t = 0 s. Movies in composite (left), membrane channel (red), Snf7 channel (green), Vps4 channel (cyan) and transmitted light (gray) are displayed. Time is reported in seconds. The bead serves as size reference (diameter 1.56 μm). Upon ATP release, the protein intensity in the tube increases. Protein puncta form in the tube that remain until the tube is severed at t = 418 s, leaving a remnant on the bead.